Mon. Not. R. Astron. Soc. (2007) doi:10.1111/j.1365-2966.2007.12016.x

Metal and molecule cooling in simulations of structure formation

U. Maio,[1⋆] K. Dolag,[1⋆] B. Ciardi[1⋆] and L. Tornatore[2⋆]
[1]*Max-Planck-Institut für Astrophysik, Karl-Schwarzschild-Strasse 1, D-85748 Garching b. München, Germany*
[2]*SISSA/ISAS, Via Beirut 4, I-34014 Trieste, Italy*

Accepted 2007 May 22. Received 2007 May 22; in original form 2007 April 17

ABSTRACT

Cooling is the main process leading to the condensation of gas in the dark matter potential wells and consequently to star and structure formation. In a metal-free environment, the main available coolants are H, He, H_2 and HD; once the gas is enriched with metals, these also become important in defining the cooling properties of the gas. We discuss the implementation in GADGET-2 of molecular and metal cooling at temperatures lower that 10^4 K, following the time-dependent properties of the gas and pollution from stellar evolution. We have checked the validity of our scheme comparing the results of some test runs with previous calculations of cosmic abundance evolution and structure formation, finding excellent agreement. We have also investigated the relevance of molecule and metal cooling in some specific cases, finding that inclusion of HD cooling results in a higher clumping factor of the gas at high redshifts, while metal cooling at low temperatures can have a significant impact on the formation and evolution of cold objects.

Key words: galaxies: formation – cosmology: theory – early Universe.

1 INTRODUCTION

The understanding of cosmic structure formation and evolution is one of the most outstanding problems in astrophysics, which requires dealing with processes on very large scales, like galactic or cluster properties and, at the same time, on very small scales, like atomic behaviour of gas and plasma. To join these extremes, it is fundamental to include atomic physics into astrophysics and cosmology. In fact, only with a unified study it was and is still possible to justify many physical phenomena otherwise not explained, like, for example, the very well-known O III forbidden line, typical of many gaseous nebulae. Interesting introductions into this subject are found in Spitzer (1978), the paper review by Osterbrock (1988) and Osterbrock (1989).

Nowadays, one of the main links between 'small scales' and 'large scales' seems to be the cooling properties of the gas as, to form cosmic structures, it is necessary for the gas to condense in the dark matter potential wells and emit energy as radiation (comprehensive reviews on the topic are Barkana & Loeb 2001; Ciardi & Ferrara 2005). For this reason it is fundamental to investigate the chemical properties of molecules and atoms and their cooling capabilities. In the standard cosmological scenario for structure formation, the first objects are supposed to form in metal-free haloes with virial temperatures lower than 10^4 K, for which atomic cooling is ineffective. In such physical conditions, the most-efficient coolants are likely to be molecules (e.g. Lepp & Shull 1984; Puy et al. 1993).

⋆E-mail: maio@mpa-garching.mpg.de (UM); kdolag@mpa-garching.mpg.de (KD); ciardi@mpa-garching.mpg.de (BC); torna@sissa.it (LT)

As hydrogen is the dominant element in the Universe, with a primordial mass fraction of about 76 per cent, we expect that the derived molecules will play a role in the cosmological gas chemistry. The first studies in this direction were made by Saslaw & Zipoy (1967) followed by Peebles & Dicke (1968) and many others (Hollenbach & McKee 1979; Abel et al. 1997; Galli & Palla 1998; Stancil, Lepp & Dalgarno 1998), who highlighted the importance of H_2 in cooling gas down to temperatures of about 10^3 K.

In addition, one should also consider that, besides hydrogen, nucleosynthesis calculations predict the existence of primordial deuterium and lithium. Recent measurements from a metal-poor damped Lyman α system (O'Meara et al. 2006) give $\log(D/H) = -4.48 \pm 0.06$ and are consistent with other observations (Burles & Tytler 1998; Pettini & Bowen 2001), while the abundance of Li (around 10^{-10}) is not very well determined and can vary by a factor of 2 or 3 when compared to the measurements in the atmospheres of old stars (Korn et al. 2006; Yong et al. 2006). Other molecules derived from Li (e.g. LiH and LiH^+) have much lower abundances (e.g. Lepp & Shull 1984; Puy et al. 1993; Galli & Palla 1998).

Another potentially interesting molecule is HD. Due to its permanent electric dipole moment,[1] HD has higher rotational transition probabilities and smaller rotational energy separations compared

[1] Some values of the permanent HD electric dipole moment found in the literature are $D = 8.3 \times 10^{-4}$ debye (Abgrall, Roueff & Viala 1982) and $D = 8.51 \times 10^{-4}$ debye (Thorson, Choi & Knudson 1985). The first data date back to McKellar, Goetz & Ramsay (1976); for a theoretical, *ab initio*, non-relativistic, perturbative treatment, via radial Schroedinger equation, see also Ford & Browne (1977), and references therein.

to H_2 and thus, despite its low abundance of $\log(HD/H_2) \sim -4.5$ (e.g. Lepp & Shull 1984; Puy et al. 1993; Galli & Palla 1998), HD can be an efficient coolant (Flower 2000; Galli & Palla 2002; Lipovka, Núñez-López & Avila-Reese 2005; Abgrall & Roueff 2006) and bring the gas in primordial haloes to temperatures of the order of 10^2 K. This results into a smaller Jeans mass and a more efficient fragmentation process. For haloes with virial temperatures in the range 10^3–10^4K, HD cooling can be as relevant as H_2, while its effects are expected to be minor for larger haloes (see Ripamonti 2007; Shchekinov & Vasiliev 2006).

The formation of primordial structures and stars has been investigated by many authors (like Bromm, Coppi & Larson 1999, 2002; Karlsson 2006; Yoshida et al. 2006) but our understanding of the problem is still limited, because we are lacking information on all those feedback effects (such as metal pollution, mass loss and energy deposition from the first stars) that profoundly affect it. In particular, it is now commonly accepted that the presence of metals, by determining the cooling (and thus fragmentation) properties of a gas, influences the shape of the initial mass function (IMF), leading to a transition from a top-heavy IMF to a Salpeter-like IMF, when a critical metallicity – varying between $\sim 10^{-6}$ and $\sim 10^{-3.5}\,Z_\odot$, according to different authors (Bromm & Loeb 2003; Schneider et al. 2003, 2006) – is reached; observationally, there are only few constraints (Frebel, Johnson & Bromm 2007).

Tornatore et al. (2004) have presented the first implementation of a detailed chemical feedback model in the numerical code GADGET [other works on this subject are Raiteri et al. (1996), Gnedin (1998), Kawata & Gibson (2003) and Ricotti & Ostriker (2004)], through which they study metal-enrichment for different feedback/IMF scenarios.

In this study, we discuss the implementation in GADGET of molecular and metal cooling at temperatures below 10^4 K and we present a scheme able to deal both with primordial and with metal-enriched composition. In details, we extend the existing implementation in GADGET of H_2 chemistry (Yoshida et al. 2003), in order to include HD, HeH^+ and metal cooling at those low temperatures. Indeed, these species are expected to be relevant for the formation and evolution of cold objects.

This paper is organized as follows. In Section 2, we describe the computations of deuterium chemistry (Section 2.1), metal lines (Section 2.2) and their cooling capabilities (Section 2.3); in Section 3, we perform tests of our numerical implementation about chemical abundance evolution (Section 3.1), cosmic structure formation (Section 3.2) and cluster evolution (Section 3.3); in Section 4, we discuss the results and give our conclusions.

2 METHODS AND TOOLS

In the commonly adopted scenario of structure formation, objects form from the collapse, shock and successive condensation of gas into clouds having a typical mass of the order of the Jeans mass. This process requires the gas to cool down, that is, the conversion of kinetic energy into radiation that eventually escapes from the system. This can occur via inelastic collisions which induce atomic electronic transitions to upper states, followed by de-excitations and emission of radiation. Details of the cooling process will depend on the type of elements considered and of transitions involved.

In a standard primordial environment, the main coolants are expected to be hydrogen, helium and some molecules like H_2 and HD; if the medium is metal-enriched, the heavier elements become important coolants, thanks to a larger number of possible atomic transitions with different energy separations.

The relevant quantity describing the cooling properties of a plasma is the energy emitted per unit time and volume, that is, the cooling function. (We will indicate it with Λ, adopting cgs units, erg cm^{-3} s^{-1}.)[2]

The characteristic time-scale for the cooling, determined by Λ, is important to discriminate whether the gas can cool during the infall phase in the dark matter gravitational potential wells: structures are able to form only if the cooling time is short enough compared to the free-fall time.

In this work, we focus on the effects of molecules and metals in gas at low temperatures. In particular, we will include their treatment in GADGET-2 (Springel, Yoshida & White 2001; Springel 2005). This code uses a tree-particle-mesh algorithm to compute the gravitational forces and implements a smoothed particle hydrodynamics (SPH) algorithm to treat the baryons. Moreover, it is possible to follow the main non-equilibrium reactions involving electrons, hydrogen, helium and H_2, with the respective ionization states (Yoshida et al. 2003). Stellar feedback processes and metal release from Type II supernova (SNII), Type Ia supernova (SNIa) and asymptotic giant branch (AGB) stars are also included together with metal cooling at temperatures higher than 10^4 K (for a detailed discussion, see Tornatore et al. 2007, and references therein).

In the following, we are going to discuss in detail our HD and metal line treatment at $T < 10^4$ K.

2.1 HD treatment

The HD molecule primarily forms through reactions between primordial deuterium and hydrogen atoms or molecules: a complete model for the evolution of HD involves 18 reactions (Nakamura & Umemura 2002) but, as their solution becomes quite computationally expensive when implemented in cosmological simulations, we use only the set of reactions selected by Galli & Palla (2002), which are the most relevant for HD evolution:

$$H_2 + D \rightarrow HD + H, \quad (1)$$

$$H_2 + D^+ \rightarrow HD + H^+, \quad (2)$$

which lead to HD formation;

$$HD + H \rightarrow D + H_2, \quad (3)$$

$$HD + H^+ \rightarrow D^+ + H_2, \quad (4)$$

for HD dissociation and H_2 formation; and

$$H^+ + D \rightarrow H + D^+, \quad (5)$$

$$H + D^+ \rightarrow H^+ + D, \quad (6)$$

for charge-exchange reactions.

From reactions (1)–(6), we see that HD abundance primarily depends on the amount of primordial deuterium and on the H_2 fraction.

For each species i, the variation in time of its number density n_i is

$$\frac{\mathrm{d}n_i}{\mathrm{d}t} = \sum_p \sum_q k_{pq,i} n_p n_q - \sum_l k_{li} n_l n_i, \quad (7)$$

where $k_{pq,i}$ in the first term on the right-hand side is the creation rate from species p and q, and k_{li} is the destruction rate from interactions

[2] Sometimes it is possible to find the same notation Λ for the cooling rate in erg cm^3 s^{-1}.

colour on web

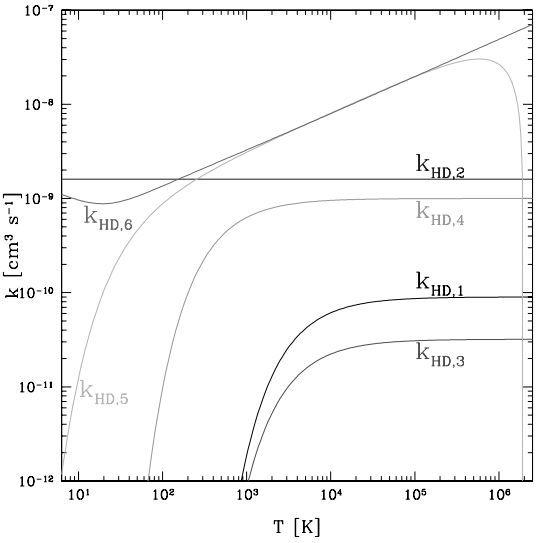

Figure 1. Temperature evolution of the reaction rates for deuterium chemistry. The labels refer to the number of the equation in the text.

of the species i with the species l; they are temperature-dependent and are usually expressed in (cm^3 s^{-1}).

A plot of the rates as a function of the temperature is given in Fig. 1, and the exact expressions and references in Appendix A. From the figure, it is clear that the most important reactions in the relevant range of temperatures are reactions (5) and (6), and that the HD creation rates of reactions (1) and (2) are always higher than the corresponding destruction rates of reactions (3) and (4), respectively.

We have also considered HeH^+ molecule evolution and found negligible effects on the cooling properties of the gas. The rates for HeH^+ formation and destruction are given in Appendix A.

We implement our chemistry model extending the code by Yoshida et al. (2003), which adopts the rates from Abel et al. (1997), and modify it for self-consistency to obtain a set of reactions including e^-, H, H^+, He, He^+, He^{++}, H_2, H_2^+, H^-, D, D^+, HD and HeH^+ (a complete list of the reactions are given in Table 1).

The set of differential equations (7) are evaluated via simple linearization, according to a backward difference formula (Anninos et al. 1997): given the time-step Δt, at each time t and for each species i, equation (7) can be re-written as

$$\frac{n_i^{t+\Delta t} - n_i^t}{\Delta t} = C_i^{t+\Delta t} - D_i^{t+\Delta t} n_i^{t+\Delta t}, \tag{8}$$

where we have introduced the creation coefficient for the species i, in (cm^{-3} s^{-1}), as

$$C_i = \sum_p \sum_q k_{pq,i} n_p n_q \tag{9}$$

and the destruction coefficient, in (s^{-1}), as

$$D_i = \sum_l k_{li} n_l. \tag{10}$$

The number density, n_i^t, is then updated from equation (8):

$$n_i^{t+\Delta t} = \frac{C_i^{t+\Delta t} \Delta t + n_i^t}{1 + D_i^{t+\Delta t} \Delta t}. \tag{11}$$

We apply this treatment to all chemical species.

Table 1. Set of reactions in the code.

Reactions	References for the rate coefficients
$H + e^- \rightarrow H^+ + 2e^-$	A97/Y06
$H^+ + e^- \rightarrow H + \gamma$	A97/Y06
$He + e^- \rightarrow He^+ + 2e^-$	A97/Y06
$He^+ + e^- \rightarrow He + \gamma$	A97/Y06
$He^+ + e^- \rightarrow He^{++} + 2e^-$	A97/Y06
$He^{++} + e^- \rightarrow He^+ + \gamma$	A97/Y06
$H + e^- \rightarrow H^- + \gamma$	A97/Y06
$H^- + H \rightarrow H_2 + e^-$	A97/Y06
$H + H^+ \rightarrow H_2^+ + \gamma$	A97/Y06
$H_2^+ + H \rightarrow H_2 + H^+$	A97/Y06
$H_2 + H \rightarrow 3H$	A97
$H_2 + H^+ \rightarrow H_2^+ + H$	S04/Y06
$H_2 + e^- \rightarrow 2H + e^-$	ST99/GB03/Y06
$H^- + e^- \rightarrow H + 2e^-$	A97/Y06
$H^- + H \rightarrow 2H + e^-$	A97/Y06
$H^- + H^+ \rightarrow 2H$	P71/GP98/Y06
$H^- + H^+ \rightarrow H_2^+ + e^-$	SK87/Y06
$H_2^+ + e^- \rightarrow 2H$	GP98/Y06
$H_2^+ + H^- \rightarrow H + H_2$	A97/Y06
$D + H_2 \rightarrow HD + H$	WS02
$D^+ + H_2 \rightarrow HD + H^+$	WS02
$HD + H \rightarrow D + H_2$	SLP98
$HD + H^+ \rightarrow D^+ + H_2$	SLP98
$H^+ + D \rightarrow H + D^+$	S02
$H + D^+ \rightarrow H^+ + D$	S02
$He + H^+ \rightarrow HeH^+ + \gamma$	RD82, GP98
$HeH^+ + H \rightarrow He + H_2^+$	KAH79, GP98
$HeH^+ + \gamma \rightarrow He + H^+$	RD82, GP98

Notes. P71 = Peterson et al. (1971); KAH79 = Karpas et al. (1979); RD82 = Roberge & Dalgarno (1982); SK87 = Shapiro & Kang (1987); A97 = Abel et al. (1997); GP98 = Galli & Palla (1998); SLP98 = Stancil et al. (1998); ST99 = Stibbe & Tennyson (1999); WS02 = Wang & Stancil (2002); S02 = Savin (2002); GB03 = Glover & Brand (2003); S04 = Savin et al. (2004); Y06 = Yoshida et al. (2006).

2.2 Metal treatment at $T < 10^4$ K

For our calculations, we consider oxygen, carbon, silicon and iron, because they are the most-abundant heavy atoms released during stellar evolution and, therefore, they play the most-important role in chemical enrichment and cooling: indeed, SNeII expel mostly oxygen and carbon, while SNeIa expel silicon and iron (Thielemann et al. 2001; Park et al. 2003; Borkowski, Hendrick & Reynolds 2004; Meynet, Ekström & Maeder 2006).

We make the common assumption that carbon, silicon and iron are completely ionized, while oxygen is neutral. This is justified because, in a cosmological context, ultraviolet (UV) radiation below 13.6 eV (from various astrophysical sources, like quasars, stars, etc.) can escape absorption by neutral hydrogen and generate a UV background that can ionize atoms with first ionization potential lower than 13.6 eV (like carbon, silicon and iron). while oxygen remains predominantly neutral since its first ionization potential of 13.62 eV is higher (see also Bromm & Loeb 2003; Santoro & Shull 2006).

As in the low-density regime of interest here thermodynamic equilibrium is never reached (see discussion of equation 16), the Boltzmann distribution for the population of atomic levels cannot be used. Thus, we will use the detailed balancing principle instead. For each level i of a given species, we impose that the number of transitions to that level (which *populate* it), per unit time and volume equals the number of transitions from the same level i to other levels

(which *depopulate* it), per unit time and volume:

$$n_i \sum_j P_{ij} = \sum_j n_j P_{ji} \quad (i \neq j). \tag{12}$$

In formula (12), P_{ij} is the probability per unit time of the transition $i \rightarrow j$ and n_i and n_j are the number densities of atoms in the ith and jth (with $i \neq j$) level. The left-hand side of the previous equation refers to depopulations of the ith level, while the right-hand side refers to the transitions which can populate it.

The probability of a given transition can be easily computed once the Einstein coefficients and the collisional rates are known.

The further constraint which must be satisfied is the number particle conservation

$$\sum_j n_j = n_{\rm tot}, \tag{13}$$

where $n_{\rm tot}$ is the total number density of the species considered and n_j the population of the generic level j.

In case of collisional events, the rate at which the transition $i \rightarrow j$ occurs is by definition

$$n_i n_x \gamma_{ij} \equiv n_i n_x \langle u \sigma_{ij} \rangle = n_i n_x \int_0^\infty u \sigma_{ij} f(u)\, {\rm d}^3 u, \tag{14}$$

where σ_{ij} is the cross-section of the process, $f(u)\ {\rm d}^3u$ is the velocity distribution function of the particles (typically a Maxwellian), γ_{ij} is the collisional rate, n_i the number density of the particles in the ith level and n_x is the colliding particle number density.

The relation between γ_{ij} and γ_{ji} is

$$g_i \gamma_{ij} = g_j \gamma_{ji} {\rm e}^{-\beta \Delta E_{ji}}, \tag{15}$$

where g_i and g_j are the level multiplicities, $\beta = (kBT)^{-1}$, ΔE_{ji} is the energy level separation and $i < j$.

In addition to collisionally induced transitions, spontaneous transitions can take place with an emission rate given by the Einstein A coefficient.

It is convenient to define the critical number density for the transition $i \rightarrow j$ as

$$n_{{\rm cr},ij} = \frac{A_{ij}}{\gamma_{ij}}. \tag{16}$$

This determines the minimum density above which thermal equilibrium can be assumed and low-density deviations from the Boltzmann distribution become irrelevant. At densities below $n_{{\rm cr},ij}$, we expect values of the excited level populations lower than that in the thermodynamic limit, because of the reduced number of interactions.[3]

For a two-level system, the low-density level populations arising from electron and hydrogen impact excitations can be found by solving the system of equations resulting from conditions (13) and (12):

$$\begin{cases} n_1 + n_2 = n_{\rm tot} \\ n_1 n_{\rm H} \gamma_{12}^{\rm H} + n_1 n_{\rm e} \gamma_{12}^{\rm e} - n_2 n_{\rm H} \gamma_{21}^{\rm H} - n_2 n_{\rm e} \gamma_{21}^{\rm e} - n_2 A_{21} = 0 \end{cases}, \tag{17}$$

where $n_{\rm H}$ and $n_{\rm e}$ are the hydrogen and electron number densities, while $\gamma_{12}^{\rm H}$ and $\gamma_{12}^{\rm e}$ are the H-impact and e-impact excitation rates.

[3] The critical number density depends on the particular line transition considered; typical values for the fine structure transitions we are mostly interested in are of the order of $\sim 10^5$ cm^{-3}.

The solution of (17) is:

$$\frac{n_1}{n_{\rm tot}} = \frac{\gamma_{21}^{\rm H} + \gamma_{21}^{\rm e} n_{\rm e}/n_{\rm H} + A_{21}/n_{\rm H}}{\gamma_{12}^{\rm H} + \gamma_{21}^{\rm H} + \left(\gamma_{12}^{\rm e} + \gamma_{21}^{\rm e}\right) n_{\rm e}/n_{\rm H} + A_{21}/n_{\rm H}} \tag{18}$$

$$\frac{n_2}{n_{\rm tot}} = \frac{\gamma_{12}^{\rm H} + \gamma_{12}^{\rm e} n_{\rm e}/n_{\rm H}}{\gamma_{12}^{\rm H} + \gamma_{21}^{\rm H} + \left(\gamma_{12}^{\rm e} + \gamma_{21}^{\rm e}\right) n_{\rm e}/n_{\rm H} + A_{21}/n_{\rm H}}. \tag{19}$$

The ratio between the two level populations

$$\frac{n_2}{n_1} = \frac{\gamma_{12}^{\rm H} + \gamma_{12}^{\rm e} n_{\rm e}/n_{\rm H}}{\gamma_{21}^{\rm H} + \gamma_{21}^{\rm e} n_{\rm e}/n_{\rm H} + A_{21}/n_{\rm H}} \tag{20}$$

$$\overset{n_{\rm e} \ll n_{\rm H}}{\sim} \frac{\gamma_{12}^{\rm H}}{\gamma_{21}^{\rm H} + A_{21}/n_{\rm H}} \tag{21}$$

will in general deviate from the Boltzmann statistic, because the spontaneous emission term dominates over the collisional term at low densities. In a neutral dense gas, instead, the level population saturates and simply reduces to a Boltzmann distribution, independently from the colliding particle number density.

In case of n-level systems, one must solve the $n \times n$ population matrix consisting of $n - 1$ independent balancing equations (12) and the constraint of particle conservation (13).

In the modelling, we approximate C II and Si II as two-level systems, and O I and Fe II as five-level systems (Santoro & Shull 2006).

Further details on the atomic data and structures are reported in Appendix B.

2.3 Cooling

In addition to calculating the chemical evolution of the gas, we need to evaluate the cooling induced by different species. In the original code, hydrogen and helium cooling from collisional ionization, excitation and recombination (Hui & Gnedin 1997), Compton cooling/heating and Bremsstrahlung (Black 1981) are evaluated. For the H_2 and H_2^+ cooling, the rates quoted in Galli & Palla (1998) are adopted. We take the HD cooling function from Lipovka et al. (2005), who consider the HD ro-vibrational structure and perform calculations for $J \leqslant 8$ rotational levels and $v = 0, 1, 2, 3$ vibrational levels. Their results are somehow more accurate than other approximations (Flower 2000; Galli & Palla 2002) and valid for a wide range of number densities (up to 10^4 cm^{-3}) and temperatures (10^2–2×10^4 K).

In Fig. 2, we show cooling functions for H_2, HD and H_2^+ molecules; for the latter case, we distinguish between neutral hydrogen impact and electron impact cooling; we have assumed fractions $x_{\rm HD} = 10^{-8}, x_{\rm H_2} = 10^{-5}, x_{\rm H_2^+} = 10^{-13}, x_{\rm e^-} = 10^{-4}$ and a total hydrogen number density $n_{\rm H} = 1$ cm^{-3}. Due to its very low abundance, H_2^+ is less effective than neutral H_2 and HD, which remain the only relevant coolants over the plotted range of temperature.

We highlight that the contribution of HD to gas cooling at low temperatures is dominant in the case considered here, but its relevance strongly depends on the relative abundances of the species.

The cooling for metal line transitions is computed as follows. In case of two-level systems, we define

$$\Lambda \equiv n_2 A_{21} \Delta E_{21}, \tag{22}$$

where n_2 is the atomic excited state number density, A_{21} is the probability per unit time of the transition $2 \rightarrow 1$ and ΔE_{21} is the energy separation of the levels.

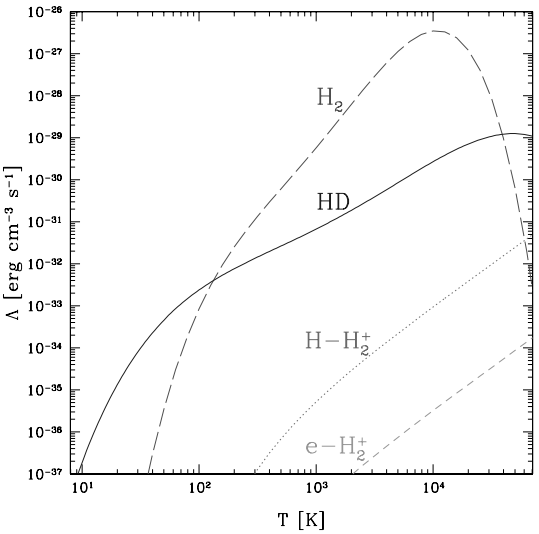

Figure 2. Cooling functions for a primordial gas with a hydrogen number density of 1 cm^{-3} and the following fractions for the different species: $x_{\mathrm{HD}} = 10^{-8}, x_{\mathrm{H}_2} = 10^{-5}, x_{\mathrm{H}_2^+} = 10^{-13}$ and $x_{\mathrm{e}^-} = 10^{-4}$. The H_2 cooling function (long-dashed line) is plotted together with the HD (solid line), H-impact H_2^+ (dotted line) and e-impact H_2^+ (short-dashed line) cooling functions. The fits for H_2^+ cooling are appropriate only for $T < 10^4$ K.

Combining equations (19) and (22), one can write the previous equation as a function only of the total number density of the species:

$$\Lambda = \frac{\gamma_{12}^{\mathrm{H}} + \gamma_{12}^{\mathrm{e}} n_{\mathrm{e}}/n_{\mathrm{H}}}{\gamma_{12}^{\mathrm{H}} + \gamma_{21}^{\mathrm{H}} + \left(\gamma_{12}^{\mathrm{e}} + \gamma_{21}^{\mathrm{e}}\right) n_{\mathrm{e}}/n_{\mathrm{H}} + A_{21}/n_{\mathrm{H}}} n_{\mathrm{tot}} A_{21} \Delta E_{21}. \quad (23)$$

For $n_{\mathrm{e}} \ll n_{\mathrm{H}}$, the previous formula is consistent with the one quoted in Santoro & Shull (2006), who do not consider electron impact excitation effects. Using equations (20) and (16), Λ can also be written as a function of the fundamental level population:

$$\Lambda = \frac{n_1 n_{\mathrm{H}} \gamma_{12}^{\mathrm{H}} + n_1 n_{\mathrm{e}} \gamma_{12}^{\mathrm{e}}}{n_{\mathrm{H}}/n_{\mathrm{cr},21}^{\mathrm{H}} + n_e/n_{\mathrm{cr},21}^{\mathrm{e}} + 1} \Delta E_{21} \quad (24)$$

$$\overset{n_{\mathrm{e}} \ll n_{\mathrm{H}}}{\sim} \frac{n_1 n_{\mathrm{H}} \gamma_{12}^{\mathrm{H}}}{n_{\mathrm{H}}/n_{\mathrm{cr},21}^{\mathrm{H}} + 1} \Delta E_{21} \quad (25)$$

where $n_{\mathrm{cr},21}^{\mathrm{H}}$ and $n_{\mathrm{cr},21}^{\mathrm{e}}$ being the critical density for the transition $2 \rightarrow 1$ due to H- and e-impact excitations, respectively.

In particular, in the low-density limit ($n_{\mathrm{H,e}} \ll n_{\mathrm{cr}}$), the above equation becomes

$$\Lambda \simeq \left[n_1 n_{\mathrm{H}} \gamma_{12}^{\mathrm{H}} + n_1 n_{\mathrm{e}} \gamma_{12}^{\mathrm{e}}\right] \Delta E_{21} \quad (26)$$

$$\overset{n_{\mathrm{e}} \ll n_{\mathrm{H}}}{\sim} n_1 n_{\mathrm{H}} \gamma_{12}^{\mathrm{H}} \Delta E_{21}. \quad (27)$$

In this regime, each excitation – see formulae (26) and (27) – is statistically followed by emission of radiation – see the general definition (22).

In the high-density limit, one finds the expected thermodynamic equilibrium cooling rate

$$\Lambda \simeq \frac{g_2}{g_1} \mathrm{e}^{-\beta \Delta E_{21}} n_1 \frac{A_{21}}{1 + n_{\mathrm{e}} \gamma_{21}^{\mathrm{e}}/n_{\mathrm{H}} \gamma_{21}^{\mathrm{H}}} \Delta E_{21} + \frac{g_2}{g_1} \mathrm{e}^{-\beta \Delta E_{21}} n_1 \frac{A_{21}}{1 + n_{\mathrm{H}} \gamma_{21}^{\mathrm{H}}/n_{\mathrm{e}} \gamma_{21}^{\mathrm{e}}} \Delta E_{21} \quad (28)$$

$$\overset{n_{\mathrm{e}} \ll n_{\mathrm{H}}}{\sim} \frac{g_2}{g_1} \mathrm{e}^{-\beta \Delta E_{21}} n_1 A_{21} \Delta E_{21}. \quad (29)$$

In the right-hand side, it is easy to recognize the Boltzmann distribution of populations for n_2. It is interesting to note that the cooling function does not depend any more on the number density of the colliding particles, but only on the species abundance, in contrast with the low-density regime, where there is a linear dependence on both densities.

These arguments ensure that it is safe to use formula (23) to compute the gas cooling for two-level atoms.

For n-level systems, the cooling function is simply the sum of all the contributions from each transition:

$$\Lambda \equiv \sum_{i \geqslant 1} \sum_{0 \leqslant j < i} n_i A_{ij} \Delta E_{ij}. \quad (30)$$

In general, once the number density of the cooling species is fixed, we expect the cooling function to grow linearly with the colliding particle number density and eventually to saturate, converging to the Boltzmann statistic, when the critical densities are reached. We see that C II, Si II and Fe II saturate when the colliding particle number density achieves values around 10^4–10^5 cm^{-3}, while for O I we will have a double phase of saturation: the first one at $\sim 10^5\,\mathrm{cm}^{-3}$ involving the lower three states and the second one at $\sim 10^{11}\,\mathrm{cm}^{-3}$ involving the higher two states.

As an example, in Fig. 3, we show the cooling functions for a total number density 1 cm^{-3} and for each metal species $10^{-6}\,\mathrm{cm}^{-3}$; the ratio between free electrons and hydrogen is chosen to be 10^{-4}. With these values, the presence of electrons can affect the results up to 10 per cent with respect to the zero electron fraction case. We also note that all the metals contribute with similar importance to the total cooling function and the main difference in the cooling properties of the gas will depend on their detailed chemical composition.

We also plot the cooling functions for all the temperature regime we are interested in: at temperatures higher than 10^4 K, we interpolate the Sutherland and Dopita tables (Sutherland & Dopita 1993), at lower temperatures, we include metals and molecules as discussed previously. Fig. 4 shows the cooling function for different individual metal number fractions with abundances in the range 10^{-6}–10^{-3} and H_2 and HD fractions of 10^{-5} and 10^{-8},respectively. These values for H_2 and HD are fairly typical for the intergalactic medium (IGM) gas

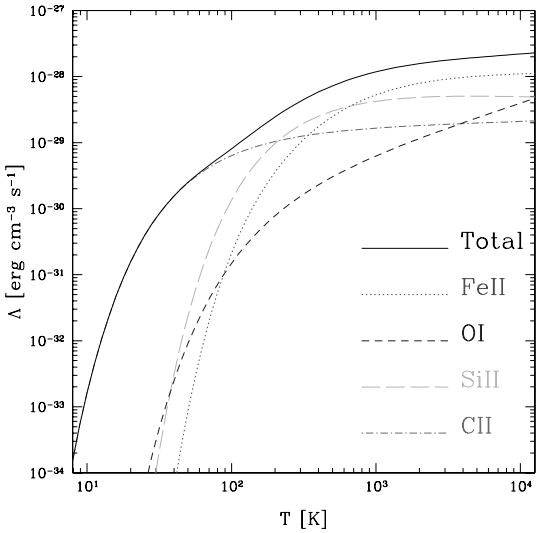

Figure 3. Cooling due to metals as a function of temperature. The computations are done for a gas with total number density of 1 cm^{-3}; for each metal species, we assume a number density of $10^{-6}\,\mathrm{cm}^{-3}$ and we set the free electron over hydrogen fraction to a value of 10^{-4}.

colour on web

colour on web

colour on web

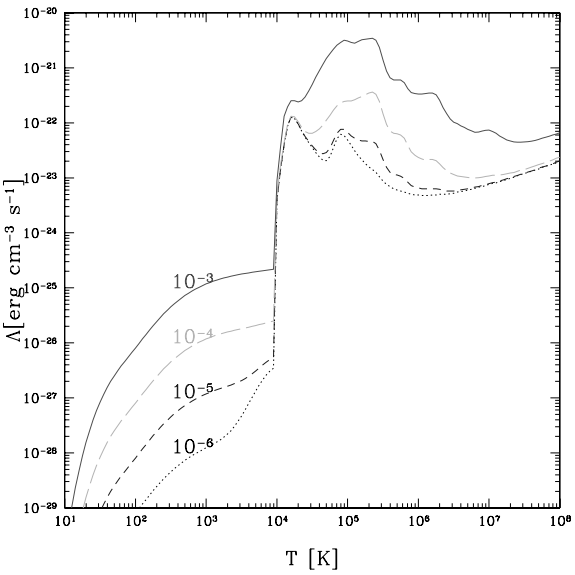

Figure 4. Total cooling due to hydrogen, helium, metals, H_2 and HD molecules as a function of temperature, for gas having a hydrogen number density of 1 cm^{-3}. The fractions of H_2 and HD are fixed to 10^{-5} and 10^{-8}, respectively. The labels in the plot refer to different amounts of metals, for individual metal number fractions of 10^{-3} (solid line), 10^{-4} (long-dashed line), 10^{-5} (short-dashed line) and 10^{-6} (dotted line).

at the mean density (see also the conclusions of Galli & Palla 1998, and references therein). In the temperature range 10^4–10^5 K, the double peak due to hydrogen and helium collisional excitations is evident at low metallicity, while it is washed out by the contribution of different metal ionization processes as the metallicity increases. For example, complete collisional ionization of carbon and oxygen produces the twin peak at 10^5 K, while complete ionization of iron is evident at about 10^7 K. At temperatures lower than 10^4 K and metal fractions lower than $\sim 10^{-6}$, the dominant cooling is given by molecules; instead, for larger metal fractions the effects of metals became dominant.

The general conclusion is that at very high redshift, when metals are not present, only H_2 and HD can be useful to cool the gas down to some 10^2 K, while after the first stars explode, ejecting heavy elements into the surrounding medium, metals quickly become the most-efficient coolants.

3 TESTS

In this section, we are going to test the implementation of HD and metal cooling using different kinds of simulations. In particular, we focus on the analysis of abundance redshift evolution, cosmic structure formation and clusters.

3.1 Abundance redshift evolution

As a first test, we investigate the behaviour of a plasma of primordial chemical composition (i.e. with no metals) looking at the redshift evolution of the single abundances. Our goal is to reproduce the results from Galli & Palla (1998), who calculate the redshift evolution of a metal-free gas at the mean density by following a detailed chemical network. For this reason, here, we perform our non-equilibrium computations on *isolated* particles, including the following chemical species: e^-, H, H^+, He, He^+, He^{++}, H_2, H_2^+, H^-, D, D^+, HD and HeH^+ and assuming a flat cosmology with no dark energy content (matter density parameter $\Omega_{0m} = 1$), baryon density parameter $\Omega_{0b} = 0.037$, Hubble constant, in units of 100 km s^{-1} Mpc^{-1}, $h = 0.67$ and initial gas temperature of 1000 K.

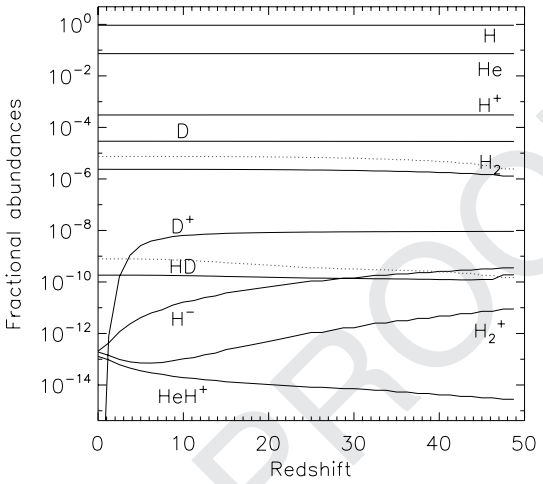

Figure 5. Abundances as a function of redshift. The solid lines refer to the abundance evolution in a flat CDM universe with $h = 0.67$, $\Omega_{0m} = 1$, $\Omega_{0b} = 0.037$; the dotted lines refer to H_2 and HD evolution in a ΛCDM model with $h = 0.73$, $\Omega_{0m} = 0.237$, $\Omega_{0\Lambda} = 0.763$ and $\Omega_{0b} = 0.041$.

colour on web

The evolution of the number fractions for the different species is plotted in Fig. 5; the electron abundance is given from charge conservation of neutral plasma and is normally very close to the H^+ value, this being the dominant ion. These results are in very good agreement with those of Galli & Palla (1998).

In our set of reactions, due to the low initial gas temperature, the collisions are inefficient to ionize helium. The inclusion of HeH^+ creation

$$\mathrm{He} + \mathrm{H}^+ \rightarrow \mathrm{HeH}^+ + \gamma \tag{31}$$

contributes to rise H_2^+ abundance mainly via reaction

$$\mathrm{HeH}^+ + \mathrm{H} \rightarrow \mathrm{He} + \mathrm{H}_2^+ \tag{32}$$

and weakly decrease the H^- number fraction via

$$\mathrm{HeH}^+ + \gamma \rightarrow \mathrm{He} + \mathrm{H}^+, \tag{33}$$

$$\mathrm{H}^+ + \mathrm{H}^- \rightarrow 2\mathrm{H}, \tag{34}$$

where γ indicates the photons. Because of the very low HeH^+ abundance reached, there is no substantial He atom abundance evolution.

Another *caveat* to take into account is the lack of reactions between D^+ and free electrons which would destroy the deuterium ions more efficiently, but without altering significantly the global amount of HD formed. We note also the exponential decay of D^+ due to the rate coefficient of equation (5) and the freezing out of H^+, H_2, D and HD number fractions.

As a comparison, we also plot (dotted lines) the H_2 and HD abundance evolution in a flat Λ cold dark matter (ΛCDM) model having $h = 0.73$, $\Omega_{0m} = 0.237$, $\Omega_{0\Lambda} = 0.763$, $\Omega_{0b} = 0.041$ (Spergel et al. 2006). The slight increment observed is due to the fact that in the CDM cosmology the baryon fraction is about 4 per cent, making the interactions among different species rarer than that in the ΛCDM model, for which the baryon fraction is about 17 per cent. In addition, the cosmological constant is dominant only at redshifts below 1. The evolution of the other species is similar in both cosmologies.

Q5

3.2 Cosmic structure formation

To test the behaviour of the code in simulations of structure formation and evolution and the impact of HD, we run a cosmological simulation with the same properties and cosmology as in Maio et al. (2006). The main difference here is the addition of HD chemistry. We adopt the concordance ΛCDM model with $h = 0.7$, $\Omega_{0m} = 0.3$, $\Omega_{0b} = 0.04$, $\Omega_{0\Lambda} = 0.7$; the power spectrum is normalized assuming a mass variance in an 8 Mpc h^{-1} radius sphere, $\sigma_8 = 0.9$, and the spectral index is chosen to be $n = 1$. We sample the cosmological field (in a periodic box of 1 Mpc comoving side length) with 324^3 dark matter particles and the same number of gas particles, having a mass of about 1040 and 160 $M_\odot$, respectively. The comoving Plummer-equivalent gravitational softening length is fixed to 0.143 kpc. This allows to resolve haloes with mass of about 10^5 $M_\odot$. The simulation starts at $z = 90$ and is stopped at $z \sim 21$.

We include the reactions involving e^-, H, H^+, He, He^+, He^{++}, H_2, H_2^+, H^-, D, D^+ and HD (here we neglect HeH^+, as it has not significant effects on the simulation) and compare the results with those of Maio et al. (2006), whose ΛCDM simulation has the same features, but the chemical set does not follow the evolution of D, D^+ and HD and does not include H_2^+ cooling.

To quantify the differences between the two runs and the efficiency of the HD cooling, we calculate the gas clumping factor, C, in the simulation box, in the following way:

$$C = \frac{\sum_i m_i \rho_i \sum_j m_j \rho_j^{-1}}{\left(\sum_k m_k\right)^2}, \qquad (35)$$

where for each SPH particle, i, we indicate with m_i its mass and with ρ_i its mass density; the indices run over all the gas particles. For the sake of comparison, we calculate C using only particles with density below a given overdensity threshold, δ_M, and we make δ_M vary in the range [100, 500].

The results are plotted in Fig. 6 for both simulations. We see that the inclusion of HD makes the clumping factor increase at all redshifts, almost independently from the density threshold. This means that the gas is, on average, denser and more clumped, with an increment of about 10 per cent at a redshift ∼22.

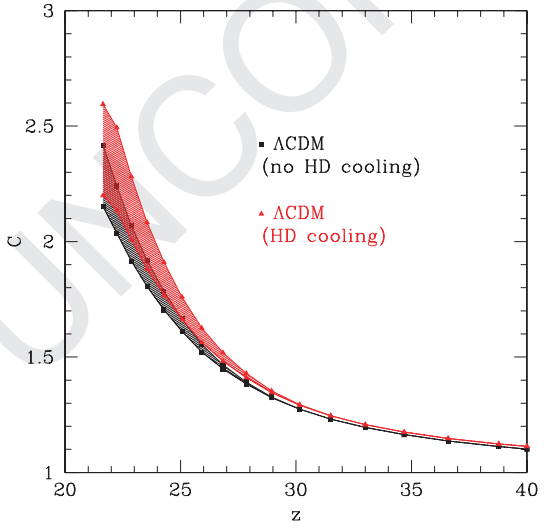

Figure 6. Gas-clumping factor as a function of redshift for two ΛCDM models with different chemical compositions. The squares refer to the clumping factor computed with standard atomic line cooling and H_2 cooling, while the triangles refer to a case which includes also HD cooling. The shaded regions correspond to the variation in the maximum overdensity between 100 (lower line in both cases) and 500 (upper line in both cases).

3.3 Cluster

So far, we have assumed either primordial gas with no metal pollution (previous test case) or a pre-defined metallicity to demonstrate the effect of the presence of metals on the cooling function at low temperature, as in Section 2.3. Now, we are going to couple our cooling function with a model for the chemical enrichment and test this implementation within a simulation that follows the formation of a cluster. In addition to testing the validity of our implementation, although there are no significant changes for the intracluster medium (ICM) to be expected, it is of interest to check whether there are regions inside the simulations where the polluted medium is cooling below 10^4 K due to its metal content.

The 'zoomed initial condition technique' (Tormen, Bouchet & White 1997) is used to extract from a dark matter only simulation with a box-size of 479 Mpc h^{-1} (we adopt a ΛCDM cosmology with $H_0 = 70\,km\,s^{-1}\,Mpc^{-1}$, $\sigma_8 = 0.9$, $\Omega_{0\Lambda} = 0.7$, $\Omega_{0m} = 0.3$ and $\Omega_{0b} = 0.04$) a smaller region and to re-simulate it at higher resolution introducing also gas particles. The cluster evolution is simulated with about 2×10^5 particles. The comoving Plummer-equivalent gravitational softening length is 5 kpc h^{-1}. At redshift zero, the selected cluster has a virial mass of about 10^{14} $M_\odot$ h^{-1}, a virial radius of about 1 Mpc h^{-1} and a virial temperature of 2×10^7 K (for more details see Dolag et al. 2004).

We start the simulation with no metallicity content. The metal abundances are then consistently derived (as in Tornatore et al. 2007) following the star formation history of the system, accounting for the lifetime of stars of different mass (Padovani & Matteucci 1993) distributed according to a Salpeter IMF and adopting appropriated stellar yields: we use those from Woosley & Weaver (1995) for massive stars (SNeII), van den Hoek & Groenewegen (1997) for low- and intermediate-mass stars and Thielemann et al. (2003) for SNeIa. The underlying subresolution model for star formation in multiphase interstellar medium (Springel & Hernquist 2003) includes a phenomenological model for feedback from galactic ejecta powered by the SNII explosions, where we have chosen the wind velocity to be 480 km s^{-1}. As we are only interested to test the effect of the metals, we exclude H_2, HD and HeH^+ chemistry and consider only atomic cooling from collisional excitations of hydrogen and helium. Once the medium gets polluted with metals, their contribution is added. For the metal cooling of the gas above 10^4 K, Sutherland and Dopita tables (Sutherland & Dopita 1993) are used. At lower temperatures, the fine structure transitions from O I, C II, Si II and Fe II are included as discussed in the previous sections.

Fig. 7 shows the cooling diagram of our simulation at redshift $z = 0$; each SPH particle is represented by a point. In the plot, different areas can be identified. The one at high temperatures (bottom right-hand panel) represents the hot ICM. When the ICM starts to get denser, cooling gets more efficient: the corresponding gas particles are represented by the points belonging to the upper branch of the cooling function and they are brought to lower and lower temperatures. Feedback from the star formation partially pushes some of them away from the cooling curve to slightly higher temperatures. Below 10^4 K, only particles which are metal-enriched can further cool down to about 300 K, while gas particles with primordial composition are stacked at 10^4 K. The three-pointed stars refer to particles within twice the virial radius and with a temperature below 8000 K, indicating that this region of the T–Λ space is also populated by gas associated with the galaxy cluster.

colour in print

colour in print

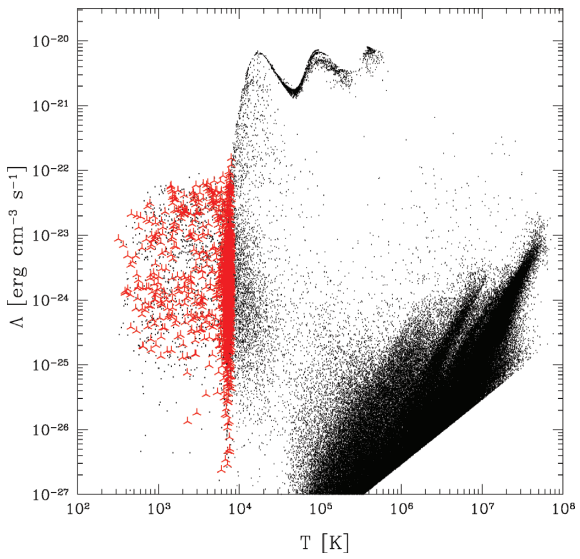

Figure 7. Distribution of the particles of a cluster simulation in the T–Λ space. The hot and thin ICM populates the bottom right-hand area. The particles within collapsed objects, which represent very dense regions of the simulation, populate the high-temperature cooling function (upper branch). In addition, metal-enriched particles undergo metal-line cooling in the low-temperature regime (below $\sim 10^4$ K). The three-pointed star symbols correspond to particles which are located within twice the virial radius of the cluster and have a temperature lower than 8000 K.

colour in print

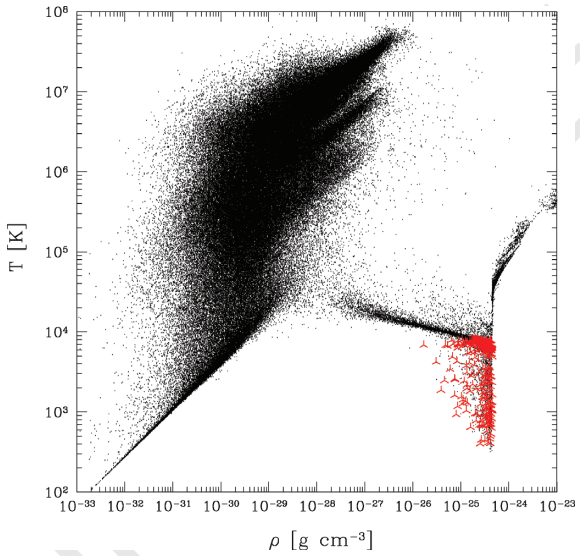

Figure 8. Distribution of the particles of a cluster simulation in the phase diagram. The hot and thin ICM populates the central left-hand area of the plot, while the dense and cooled regions of the simulation are represented in the lower right-hand part. Particles heated by feedback effects are represented by points in the central right-hand side. The three-pointed star symbols correspond to metal-enriched particles which are located within twice the virial radius of the cluster and have a temperature lower than 8000 K. We remind that the critical density of the Universe at present is $\rho_{0,\rm cr} \simeq 1.9 \times 10^{-29}\, h^2\, {\rm g\,cm^{-3}}$.

The corresponding phase diagram is shown in Fig. 8. The three-pointed star symbols are the same as in Fig. 7. The hot and thin ICM populates the central left-hand area of the plot, while the dense and cool regions occupy the lower right-hand part. Particles heated by feedback are represented by points in the central right-hand side ($\rho > 10^{-24}$ g cm^{-3}, $T > 10^5$ K). The main effect of our metal-cooling implementation is to lower the temperature of the dense medium, generating the sharp triangular area visible in the ρ–T space, at $T < 10^4$ K and $\rho > 10^{-26}$ g cm^{-3}. The points at very low densities are associated with diffuse metal-free gas; this suggests that the spread in the cooling diagram of Fig. 7 at temperature lower than 10^4 K is mainly due to different fractional metal-enrichment of the particles, rather than due to their different densities.

As already mentioned, global properties of the ICM and star formation are not significantly changed compared to the reference run without the metal line cooling from fine structure transitions. This happens because the simulation was merely meant to be a test case of the implementation of metal line cooling below 10^4 K under realistic conditions, but the haloes resolved are large enough to cool and form stars without the aid of such cooling. In order to investigate in more detail the effects of the additional cooling by molecules and metals at low temperatures on the ICM and the star formation, higher resolution simulations are needed. However, this opens interesting grounds for further investigations on the interplay between formation of small objects, with virial temperatures in the range of interest for our extended cooling function, and metal pollution from first stars.

4 CONCLUSIONS

In order to understand structure formation and evolution, a detailed study of the chemical and cooling properties of baryonic matter is needed.

In this paper, we have presented time-dependent calculations of the cooling properties of a gas in a 'low temperature' regime, using the contributions of several chemical species and we have tested the effect on cosmic structure evolution.

Hydrogen-derived molecules are effective in cooling metal-free gas below a temperature of $\sim 10^4$ K, the typical temperature range of primordial objects. On the other hand, when the medium is polluted by material expelled from stars (via SN explosions, mass losses in AGB phase and winds), metals are expected to become the main coolants.

For these reasons, we have extended previous 'non-equilibrium' calculations (Yoshida et al. 2003) in order to include in the numerical code GADGET-2 (Springel et al. 2001; Springel 2005), the deuterium chemistry and follow the formation/destruction of HD molecules. This, together with molecular hydrogen, is able to cool down the gas at $T < 10^4$ K. Thanks to its permanent electric dipole moment, HD could allow cooling even below 10^2 K (Yoshida et al. 2006).

Other molecules are not very significant for the gas cooling properties.

The treatment of metal cooling at $T \geqslant 10^4$ K is included using the tables provided by Sutherland & Dopita (1993), while the contribution from fine structure transitions of oxygen, carbon, silicon and iron at $T < 10^4$ K has been included by computing the populations of the levels, for each species, using the detailed balancing principle. More in particular, we have assumed that the UV radiation coming from the parent star ionizes carbon, silicon and iron, while oxygen remains neutral as its first ionization potential is higher than 13.6 eV. We deal with the gas radiative losses computing the detailed balancing populations of the levels due to collisional excitations arising from hydrogen and electron impacts. The cooling follows the level de-excitations. The electron impact excitations are also included, as a residual electron fraction of about 10^{-4} survives in the

post-recombination epoch and higher values are reached during the reionization process.

On the whole, we are now able to follow the evolution of e^-, H, H^+, He, He^+, He^{++}, H_2, H_2^+, H^-, D, D^+, HD, HeH^+, O, C^+, Si^+ and Fe^+; so, the code is suitable to deal both with primordial and with metal-enriched gas.

We have checked the validity of our scheme by comparing the results of some test runs with previous calculations of molecule abundance evolution, finding excellent agreement.

We have also investigated the relevance of HD and metal cooling in some specific cases.

Adding the deuterium chemistry and HD contribution to the cooling function in simulations of structure formation results in a higher clumping factor of the gas, that is, clouds are slightly denser and more compact, at high redshifts, with respect to the case when only H, He and H_2 cooling is considered. The difference is about 10 per cent at $z \sim 22$.

For what concerns the role of metal cooling at $T < 10^4$ K, we have shown that their presence is relevant in this temperature regime. In particular, in the cluster simulations we have run, fine structure transitions can actually cool the local temperature down to 10^2–10^3 K.

In conclusion, we have implemented in GADGET-2, the most-relevant features of gas cooling, in both pristine and polluted environments, for the temperature range 2.7–10^9 K. We find that HD cooling has some influence on the high-redshift gas-clumping properties, while low-temperature metal cooling has a significant impact on the formation and evolution of cold objects. In addition to investigating the above topics, this implementation can be used to study the detailed enrichment history of the IGM and its possible interplay with the transition between a primordial, massive star formation mode and a more standard one.

ACKNOWLEDGMENTS

We acknowledge profitable discussions with M. Ricotti and useful comments from G. De Lucia and the anonymous referee. UM is thankful to N. Yoshida for his helpful suggestions.

Computations were performed on the machines at the computing centre of the Max Planck Society with CPU time assigned to the Max Planck Institute for Astrophysics.

REFERENCES

Abel T., Anninos P., Zhang Y., Norman M. L., 1997, New Astron., 2, 181
Abgrall H., Roueff E., 2006, A&A, 445, 361
Abgrall H., Roueff E., Viala Y., 1982, A&AS, 50, 505
Anninos P., Zhang Y., Abel T., Norman M. L., 1997, New Astron., 2, 209
Barkana R., Loeb A., 2001, Phys. Rep., 349, 125
Black J. H., 1981, MNRAS, 197, 553
Borkowski K. J., Hendrick S. P., Reynolds S. P., 2004, 35th COSPAR Scientific Assembly Vol. 35 of COSPAR, Plenary Meeting, Supernova Ejecta in Magellanic Clouds Remnants. P. 3560
Bromm V., Loeb A., 2003, Nat, 425, 812
Bromm V., Coppi P. S., Larson R. B., 1999, ApJ, 527, L5
Bromm V., Coppi P. S., Larson R. B., 2002, ApJ, 564, 23
Burles S., Tytler D., 1998, ApJ, 507, 732
Ciardi B., Ferrara A., 2005, Space Sci. Rev., 116, 625
Dolag K., Jubelgas M., Springel V., Borgani S., Rasia E., 2004, ApJ, 606, L97
Flower D. R., 2000, MNRAS, 318, 875
Ford A. L., Browne J. C., 1977, Phys. Rev. A, 16, 1992
Frebel A., Johnson J. L., Bromm V., 2007, preprint
Galli D., Palla F., 1998, A&A, 335, 403
Galli D., Palla F., 2002, P&SS, 50, 1197
Glover S. C. O., Brand P. W. J. L., 2003, MNRAS, 340, 210
Gnedin N. Y., 1998, MNRAS, 294, 407
Hollenbach D., McKee C. F., 1979, ApJS, 41, 555
Hollenbach D., McKee C. F., 1989, ApJ, 342, 306
Hui L., Gnedin N. Y., 1997, MNRAS, 292, 27
Karlsson T., 2006, ApJ, 641, L41
Karpas Z., Anicich V., Huntress W. T. Jr, 1979, J. Chem. Phys., 70, 2877
Kawata D., Gibson B. K., 2003, MNRAS, 340, 908
Korn A. J., Grundahl F., Richard O., Barklem P. S., Mashonkina L., Collet R., Piskunov N., Gustafsson B., 2006, Nat, 442, 657
Lepp S., Shull J. M., 1984, ApJ, 280, 465
Lipovka A., Núñez-López R., Avila-Reese V., 2005, MNRAS, 361, 850
Maio U., Dolag K., Meneghetti M., Moscardini L., Yoshida N., Baccigalupi C., Bartelmann M., Perrotta F., 2006, MNRAS, 373, 869
McKellar A. R. W., Goetz W., Ramsay D. A., 1976, ApJ, 207, 663
Meynet G., Ekström S., Maeder A., 2006, A&A, 447, 623
Nakamura F., Umemura M., 2002, ApJ, 569, 549
O'Meara J. M., Burles S., Prochaska J. X., Prochter G. E., Bernstein R. A., Burgess K. M., 2006, ApJ, 649, L61
Osterbrock D. E., 1988, Publ. Astron. Soc. Pac., 100, 412
Osterbrock D. E., 1989, Astrophysics of Gaseous Nebulae and Active Galactic Nuclei. University Science Books, Mill Valley, CA
Padovani P., Matteucci F., 1993, ApJ, 416, 26
Park S., Hughes J. P., Burrows D. N., Slane P. O., Nousek J. A., Garmire G. P., 2003, ApJ, 598, L95
Peebles P. J. E., Dicke R. H., 1968, ApJ, 154, 891
Peterson J. R., Aberth W. H., Moseley J. T., Sheridan J. R., 1971, Phys. Rev. A, 3, 1651
Pettini M., Bowen D. V., 2001, ApJ, 560, 41
Puy D., Alecian G., Le Bourlot J., Leorat J., Pineau Des Forets G., 1993, A&A, 267, 337
Raiteri C. M., Villata M., Navarro J. F., 1996, A&A, 315, 105
Ricotti M., Ostriker J. P., 2004, MNRAS, 350, 539
Ripamonti E., 2007, preprint
Roberge W., Dalgarno A., 1982, ApJ, 255, 489
Santoro F., Shull J. M., 2006, ApJ, 643, 26
Saslaw W. C., Zipoy D., 1967, Nat, 216, 976
Savin D. W., 2002, ApJ, 566, 599
Savin D. W., Krstić P. S., Haiman Z., Stancil P. C., 2004, ApJ, 606, L167
Schneider R., Ferrara A., Salvaterra R., Omukai K., Bromm V., 2003, Nat, 422, 869
Schneider R., Omukai K., Inoue A. K., Ferrara A., 2006, MNRAS, 369, 1437
Shapiro P. R., Kang H., 1987, ApJ, 318, 32
Shchekinov Y. A., Vasiliev E. O., 2006, MNRAS, 368, 454
Spitzer L., 1978, Physical Processes in the Interstellar Medium. Wiley-Interscience, New York
Springel V., 2005, MNRAS, 364, 1105
Springel V., Hernquist L., 2003, MNRAS, 339, 289
Springel V., Yoshida N., White S. D. M., 2001, New Astron., 6, 79
Stancil P. C., Lepp S., Dalgarno A., 1998, ApJ, 509, 1
Stibbe D. T., Tennyson J., 1999, ApJ, 513, L147
Sutherland R. S., Dopita M. A., 1993, ApJS, 88, 253
Thielemann F.-K. et al., 2001, in Livio M., Panagia N., Sahu K., eds, Supernovae and Gamma-Ray Bursts: the Greatest Explosions since the Big Bang Abundances from Supernovae. P. 258
Thielemann F.-K. et al., 2003, Nucl. Phys. A, 718, 139
Thorson W. R., Choi J. H., Knudson S. K., 1985, Phys. Rev. A, 31, 22
Tormen G., Bouchet F. R., White S. D. M., 1997, MNRAS, 286, 865
Tornatore L., Borgani S., Matteucci F., Recchi S., Tozzi P., 2004, MNRAS, 349, L19
Tornatore L., Borgani S., Dolag K., Matteucci F.2007, MNRAS, submitted
van den Hoek L. B., Groenewegen M. A. T., 1997, A&AS, 123, 305
Wang J. G., Stancil P. C., 2002, Physica Scripta Volume T, 96
Woosley S. E., Weaver T. A., 1995, ApJS, 101, 181

Yong D., Carney B. W., Aoki W., McWilliam A., Schuster W. J., 2006, in Kubono S., Aoki W., Kajino T., Motobayashi T., Nomoto K., eds, AIP Conf. Proc. 847, Origin of Matter and Evolution of Galaxies Lithium Abundances in Halo Subgiants. P., 21
Yoshida N., Abel T., Hernquist L., Sugiyama N., 2003, ApJ, 592, 645
Yoshida N., Oh S. P., Kitayama T., Hernquist L., 2006, preprint
Yoshida N., Omukai K., Hernquist L., Abel T., 2006, ApJ, 652, 6

APPENDIX A: CHEMICAL RATES

We consider the following set of equations involving HD creation and destruction:

$$H_2 + D \rightarrow HD + H, \quad \text{(A1)}$$

$$H_2 + D^+ \rightarrow HD + H^+, \quad \text{(A2)}$$

$$HD + H \rightarrow D + H_2, \quad \text{(A3)}$$

$$HD + H^+ \rightarrow D^+ + H_2, \quad \text{(A4)}$$

$$H^+ + D \rightarrow H + D^+, \quad \text{(A5)}$$

$$H + D^+ \rightarrow H^+ + D. \quad \text{(A6)}$$

We use the rate coefficients from Wang & Stancil (2002):

$$k_{HD,1} = 9.0 \times 10^{-11} e^{-3876/T} \ cm^3 \ s^{-1}, \quad \text{(A7)}$$

$$k_{HD,2} = 1.6 \times 10^{-9} \ cm^3 \ s^{-1}, \quad \text{(A8)}$$

from Stancil et al. (1998):

$$k_{HD,3} = 3.2 \times 10^{-11} e^{-3624/T} \ cm^3 \ s^{-1}, \quad \text{(A9)}$$

$$k_{HD,4} = 10^{-9} e^{-464/T} \ cm^3 \ s^{-1}, \quad \text{(A10)}$$

and from Savin (2002):

$$k_{HD,5} = 2 \times 10^{-10} T^{0.402} e^{-37.1/T} - 3.31 \times 10^{-17} T^{1.48} \ cm^3 \ s^{-1}, \quad \text{(A11)}$$

$$k_{HD,6} = 2.06 \times 10^{-10} T^{0.396} e^{-33.0/T} + 2.03 \times 10^{-9} T^{-0.332} \ cm^3 \ s^{-1}. \quad \text{(A12)}$$

We consider the main equations for HeH^+ formation and evolution (Galli & Palla 1998), namely,

$$He + H^+ \rightarrow HeH^+ + \gamma, \quad \text{(A13)}$$

$$HeH^+ + H \rightarrow He + H_2^+, \quad \text{(A14)}$$

$$HeH^+ + \gamma \rightarrow He + H^+, \quad \text{(A15)}$$

and the rates from Roberge & Dalgarno (1982):

$$k_{HeH^+,1} = \begin{cases} 7.6 \times 10^{-18} T^{-0.5} \ cm^3 \ s^{-1}, & T \leqslant 10^3 \ K \\ 3.45 \times 10^{-16} T^{-1.06} \ cm^3 \ s^{-1}, & T > 10^3 \ K \end{cases}, \quad \text{(A16)}$$

from Karpas, Anicich & Huntress (1979):

$$k_{HeH^+,2} = 9.1 \times 10^{-10} \ cm^3 \ s^{-1} \quad \text{(A17)}$$

and from Roberge & Dalgarno (1982):

$$k_{HeH^+,3} = 6.8 \times 10^{-1} T_r^{1.5} e^{-22750/T_r} \ s^{-1}. \quad \text{(A18)}$$

In the previous expressions, T stands for the gas temperature and T_r for the radiation temperature.

APPENDIX B: ATOMIC DATA

In the following, the atomic data adopted in this paper are provided (see also Osterbrock 1989; Hollenbach & McKee 1989; Santoro & Shull 2006). We will use the usual spectroscopic notation for many electron atoms: $\boldsymbol{S}$ is the total electronic spin quantum operator, $\boldsymbol{L}$ the total electronic orbital angular momentum operator and $\boldsymbol{J} = \boldsymbol{L} + \boldsymbol{S}$ is the sum operator; $\boldsymbol{S}$, $\boldsymbol{L}$ and $\boldsymbol{J}$ are the respective quantum numbers and X indicates the orbitals s, p, d, f, ..., according as $\boldsymbol{L} = 0, 1, 2, 3, \ldots$, respectively; ${}^{2S+1}X_J$ will then indicate the atomic orbital X, with the spin quantum number $\boldsymbol{S}$ and total angular momentum quantum number $\boldsymbol{J}$; its multiplicity is equal to $2\boldsymbol{J} + 1$.

In the following, we are going to discuss the models adopted for each species and the lines considered in a more detailed way.

We will often use the notation $T_{100} = T/100 \ K$.

(i) C II. We model C II as a two-level system considering the fine structure transition $(2p)[^2P_{3/2} - {}^2P_{1/2}]$ between the quantum number $J = 3/2$ and 1/2 states. Data were taken from Hollenbach & McKee (1989):

$$\gamma_{21}^H = 8 \times 10^{-10} T_{100}^{0.07} \ cm^3 \ s^{-1};$$

$$\gamma_{21}^e = 2.8 \times 10^{-7} T_{100}^{-0.5} \ cm^3 \ s^{-1};$$

$$A_{21} = 2.4 \times 10^{-6} \ s^{-1};$$

$$\Delta E_{21} = 1.259 \times 10^{-14} \ erg \quad (T_{exc} = 91.2 \ K, \lambda = 157.74 \ \mu m).$$

The cooling function is computed according to formula (23).

(ii) Si II. We model Si II as a two-level system with the fine structure transition $(3p)[^2P_{3/2} - {}^2P_{1/2}]$. Data were taken from Hollenbach & McKee (1989):

$$\gamma_{21}^H = 8 \times 10^{-10} T_{100}^{-0.07} \ cm^3 \ s^{-1};$$

$$\gamma_{21}^e = 1.7 \times 10^{-6} T_{100}^{-0.5} \ cm^3 \ s^{-1};$$

$$A_{21} = 2.1 \times 10^{-4} \ s^{-1};$$

$$\Delta E_{21} = 5.71 \times 10^{-14} \ erg \quad (T_{exc} = 413.6 \ K, \lambda = 34.8 \ \mu m).$$

The cooling function is computed following formula (23).

(iii) O I. Neutral oxygen is a metastable system formed by the ($S = 0$, $L = 0$, 2) triplet and ($S = 1$, $L = 1$) doublet, $(2p)[^3P_2 - {}^3P_1 - {}^3P_0 - {}^1D_2 - {}^1S_0]$, in order of increasing level, with the following excitation rates (Hollenbach & McKee 1989; Santoro & Shull 2006):

$$\gamma_{21}^H = 9.2 \times 10^{-11} T_{100}^{0.67} \ cm^3 \ s^{-1};$$

$$\gamma_{31}^H = 4.3 \times 10^{-11} T_{100}^{0.80} \ cm^3 \ s^{-1};$$

$$\gamma_{32}^H = 1.1 \times 10^{-10} T_{100}^{0.44} \ cm^3 \ s^{-1};$$

$$\gamma_{41}^H = \gamma_{42}^H = \gamma_{43}^H = 10^{-12} \ cm^3 \ s^{-1};$$

$$\gamma_{51}^H = \gamma_{52}^H = \gamma_{53}^H = 10^{-12} \ cm^3 \ s^{-1};$$

$$\gamma_{21}^e = 1.4 \times 10^{-8} \ cm^3 \ s^{-1};$$

$$\gamma_{31}^e = 1.4 \times 10^{-8} \ cm^3 \ s^{-1};$$

$$\gamma_{32}^e = 5.0 \times 10^{-9} \ cm^3 \ s^{-1};$$

$$\gamma_{41}^e = \gamma_{42}^e = \gamma_{43}^e = 10^{-10} \ cm^3 \ s^{-1};$$

$$\gamma_{51}^e = \gamma_{52}^e = \gamma_{53}^e = 10^{-10} \ cm^3 \ s^{-1}.$$

The radiative transition probabilities are (Hollenbach & McKee 1989; Osterbrock 1989)

$A_{21} = 8.9 \times 10^{-5}\,\mathrm{s}^{-1}$

$A_{31} = 1.0 \times 10^{-10}\,\mathrm{s}^{-1}$;

$A_{32} = 1.7 \times 10^{-5}\,\mathrm{s}^{-1}$;

$A_{41} = 6.3 \times 10^{-3}\,\mathrm{s}^{-1}$;

$A_{42} = 2.1 \times 10^{-3}\,\mathrm{s}^{-1}$;

$A_{43} = 7.3 \times 10^{-7}\,\mathrm{s}^{-1}$;

$A_{51} = 2.9 \times 10^{-4}\,\mathrm{s}^{-1}$;

$A_{52} = 7.3 \times 10^{-2}\,\mathrm{s}^{-1}$;

$A_{54} = 1.2\,\mathrm{s}^{-1}$;

energy separations are derived from Hollenbach & McKee (1989):

$\Delta E_{21} = 3.144 \times 10^{-14}$ erg ($T_{\rm exc} = 227.7$ K, $\lambda = 63.18$ μm);

$\Delta E_{32} = 1.365 \times 10^{-14}$ erg ($T_{\rm exc} = 98.8$ K, $\lambda = 145.5$ μm);

$\Delta E_{43} = 3.14 \times 10^{-12}$ erg ($T_{\rm exc} = 2.283 \times 10^4$ K, $\lambda = 6300$ Å);

$\Delta E_{53} = 3.56 \times 10^{-12}$ erg ($T_{\rm exc} = 2.578 \times 10^4$ K, $\lambda = 5577$ Å).

To compute the cooling function, we solve for the five-level populations and sum over the contributions from each of them.

(iv) Fe II. We adopt a model for a five-level system including the transitions (3d)[$^6D_{9/2}$–$^6D_{7/2}$–$^6D_{5/2}$–$^6D_{3/2}$–$^6D_{1/2}$] in order of increasing level. For the data see also Santoro & Shull (2006) and references therein:

$\gamma_{21}^{\rm H} = 9.5 \times 10^{-10}\,\mathrm{cm}^3\,\mathrm{s}^{-1}$;

$\gamma_{32}^{\rm H} = 4.7 \times 10^{-10}\,\mathrm{cm}^3\,\mathrm{s}^{-1}$;

$\gamma_{43}^{\rm H} = 5. \times 10^{-10}\,\mathrm{cm}^3\,\mathrm{s}^{-1}$;

$\gamma_{54}^{\rm H} = 5 \times 10^{-10}\,\mathrm{cm}^3\,\mathrm{s}^{-1}$;

$\gamma_{31}^{\rm H} = 5.7 \times 10^{-10}\,\mathrm{cm}^3\,\mathrm{s}^{-1}$;

$\gamma_{41}^{\rm H} = 5 \times 10^{-10}\,\mathrm{cm}^3\,\mathrm{s}^{-1}$;

$\gamma_{51}^{\rm H} = 5 \times 10^{-10}\,\mathrm{cm}^3\,\mathrm{s}^{-1}$;

$\gamma_{42}^{\rm H} = 5 \times 10^{-10}\,\mathrm{cm}^3\,\mathrm{s}^{-1}$;

$\gamma_{52}^{\rm H} = 5 \times 10^{-10}\,\mathrm{cm}^3\,\mathrm{s}^{-1}$;

$\gamma_{53}^{\rm H} = 5 \times 10^{-10}\,\mathrm{cm}^3\,\mathrm{s}^{-1}$;

$\gamma_{21}^{\rm e} = 1.8 \times 10^{-6} T_{100}^{-0.5}\,\mathrm{cm}^3\,\mathrm{s}^{-1}$;

$\gamma_{32}^{\rm e} = 8.7 \times 10^{-7} T_{100}^{-0.5}\,\mathrm{cm}^3\,\mathrm{s}^{-1}$;

$\gamma_{43}^{\rm e} = 10^{-5} T^{-0.5}\,\mathrm{cm}^3\,\mathrm{s}^{-1}$;

$\gamma_{54}^{\rm e} = 10^{-5} T^{-0.5}\,\mathrm{cm}^3\,\mathrm{s}^{-1}$;

$\gamma_{31}^{\rm e} = 1.8 \times 10^{-6} T_{100}^{-0.5}\,\mathrm{cm}^3\,\mathrm{s}^{-1}$;

$\gamma_{41}^{\rm e} = 10^{-5} T^{-0.5}\,\mathrm{cm}^3\,\mathrm{s}^{-1}$;

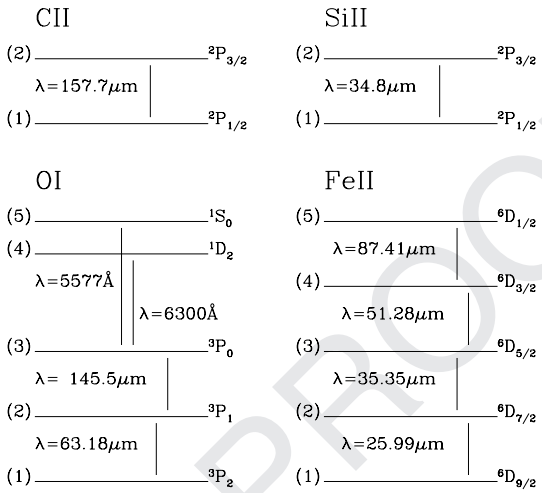

Figure B1. A scheme of the level models adopted for the different atoms with respective line-transition data.

$\gamma_{51}^{\rm e} = 10^{-5} T^{-0.5}\,\mathrm{cm}^3\,\mathrm{s}^{-1}$;

$\gamma_{42}^{\rm e} = 10^{-5} T^{-0.5}\,\mathrm{cm}^3\,\mathrm{s}^{-1}$;

$\gamma_{52}^{\rm e} = 10^{-5} T^{-0.5}\,\mathrm{cm}^3\,\mathrm{s}^{-1}$;

$\gamma_{53}^{\rm e} = 10^{-5} T^{-0.5}\,\mathrm{cm}^3\,\mathrm{s}^{-1}$;

we assume a fiducial normalization of 10^{-5} for missing data on e-impact rates. We have checked that the level populations are almost insensitive to the adopted values.

$A_{21} = 2.13 \times 10^{-3}\,\mathrm{s}^{-1}$;

$A_{32} = 1.57 \times 10^{-3}\,\mathrm{s}^{-1}$;

$A_{31} = 1.50 \times 10^{-9}\,\mathrm{s}^{-1}$;

$A_{43} = 7.18 \times 10^{-4}\,\mathrm{s}^{-1}$;

$A_{54} = 1.88 \times 10^{-4}\,\mathrm{s}^{-1}$;

$\Delta E_{21} = 7.64 \times 10^{-14}$ erg ($T_{\rm exc} = 553.58$ K, $\lambda = 25.99$ μm);

$\Delta E_{32} = 5.62 \times 10^{-14}$ erg ($T_{\rm exc} = 407.01$ K, $\lambda = 35.35$ μm);

$\Delta E_{43} = 3.87 \times 10^{-14}$ erg ($T_{\rm exc} = 280.57$ K, $\lambda = 51.28$ μm);

$\Delta E_{54} = 2.27 \times 10^{-14}$ erg ($T_{\rm exc} = 164.60$ K, $\lambda = 87.41$ μm).

To compute the cooling function, we solve for the five-level populations and sum over the contributions from each of them.

A scheme of the atomic states, with wavelengths of the transitions between different levels, is given in Fig. B1.

This paper has been typeset from a TEX/LATEX file prepared by the author.

QUERIES

Journal: MNRAS
Paper: mnr12016

Dear Author

During the copy-editing of your paper, the following queries arose. Please respond to these by marking up your proofs with the necessary changes/additions. Please write your answers on the query sheet if there is insufficient space on the page proofs. Please write clearly and follow the conventions shown on the corrections sheet. If returning the proof by fax do not write too close to the paper's edge. Please remember that illegible mark-ups may delay publication.

Query Reference	Query	Remarks
Q1	Author: To check that we have your surnames correctly identified and tagged (e.g. for indexing), we have coloured green the names that we have assumed are surnames. If any of these are wrong, please let us know so we can amend the tagging.	
Q2	Author: Please note that computer software/programming languages must be styled in SMALL CAPITAL LETTERS, according to journal style. Please check and correct this paper accordingly.	
Q3	Author: Please check the edit.	
Q4	Author: Please check the figures in the PDF proof carefully.	
Q5	Author: The reference corresponding to the citation 'Spergel et al. 2006' is not present in the references list. Please check and suggest.	
Q6	Author: Please provide complete information [editor name(s), publisher name and location] for the reference and also check the reference for correctness.	
Q7	Author: Please update the reference.	
Q8	Author: Please check the 'journal title' of this reference for correctness.	

Query Reference	Query	Remarks
Q9	Author: Please check the reference for correctness and completeness.	
Q10	Author: Please update the reference.	
Q11	Author: Please provide complete information (publisher name and location) for the reference and also check the reference for correctness.	
Q12	Author: Please update the reference.	
Q13	Author: Please provide complete information (volume or page number) for the reference and also check the reference for correctness.	
Q14	Author: Please provide complete information (publisher name and location) for the reference and also check the reference for correctness.	
Q15	Author: Please update the reference.	
Q16	Author: Journal style rules state that vectors and tensors must be written in bold italic ($\boldsymbol{X}$), matrices must be written in bold san serif ($\mathbf{X}$) and scalars must be written in italic (X). Please check carefully that the notation used throughout this paper is correct.	
Q17	Author: Please check the edit.	

MARKED PROOF

Please correct and return this set

Please use the proof correction marks shown below for all alterations and corrections. If you wish to return your proof by fax you should ensure that all amendments are written clearly in dark ink and are made well within the page margins.

Instruction to printer	*Textual mark*	*Marginal mark*
Leave unchanged	··· under matter to remain	New matter followed by or or
Insert in text the matter indicated in the margin		
Delete	through single character, rule or underline or through all characters to be deleted	or
Substitute character or substitute part of one or more word(s)	through letter or through characters	new character or new characters
Change to italics	under matter to be changed	
Change to capitals	under matter to be changed	
Change to small capitals	under matter to be changed	
Change to bold type	under matter to be changed	
Change to bold italic	under matter to be changed	
Change to lower case	Encircle matter to be changed	
Change italic to upright type	(As above)	
Change bold to non-bold type	(As above)	
Insert 'superior' character	through character or where required	or under character e.g. or
Insert 'inferior' character	(As above)	over character e.g.
Insert full stop	(As above)	
Insert comma	(As above)	
Insert single quotation marks	(As above)	or and/or or
Insert double quotation marks	(As above)	or and/or or
Insert hyphen	(As above)	
Start new paragraph		
No new paragraph		
Transpose		
Close up	linking characters	
Insert or substitute space between characters or words	through character or where required	
Reduce space between characters or words	between characters or words affected	